Accepted in SPIE Proceedings (2004)

# Electronic Charge Transport in Sapphire Studied by Optical-Pump/THz-Probe Spectroscopy

F. Wang,[1] J. Shan,[1,2] E. Knoesel,[1,3] M. Bonn,[4] and T. F. Heinz[1]
[1] Departments of Physics and Electrical Engineering, Columbia University
538 West 120 Street, New York, NY 10027
[2] Current Address: Department of Physics, Case Western Reserve University
10900 Euclid Avenue, Cleveland, OH 44106
[3] Current Address: Department of Physics, Rowan University
201 Mulica Hill Road, Glassboro, NJ 08028
[4] Leiden Institute of Chemistry, P.O. Box 9502, 2300 Leiden, The Netherlands

## ABSTRACT

THz time-domain spectroscopy (THz TDS) with ultrafast photo-excitation is applied to probe the complex conductivity of the charge carriers in sapphire over the temperature range of 40 – 350 *K*. A comparison of the measured complex conductivity to the Drude model yields the carrier scattering rate and density. The dependence of the carrier scattering rate on temperature and sample purity is used to identify the scattering mechanisms in sapphire. In the higher temperature range, scattering is determined by intrinsic phonon processes, but impurity scattering becomes dominant at low temperatures in typical optical-grade samples. In high-purity samples, however, impurity scattering remains negligible down to 40 *K*, and carrier mobilities exceeding 10,000 $cm^2/Vs$ can be achieved.

**Keywords:** Ultrafast phenomena, spectroscopy, far infrared, terahertz

## 1. INTRODUCTION

Terahertz time-domain spectroscopy (THz TDS) in conjunction with pump-probe measurements offers a powerful tool to examine charge transport and ultrafast carrier dynamics in condensed matter [1-3]. The THz spectral range provides a high degree of sensitivity to charge carriers, which even at modest concentrations generally dominate the material response. In addition, method of THz TDS yields directly information on the real and imaginary parts of the complex conductivity of the material over a spectral range extending up to a few THz. The approach involves only propagating electromagnetic waves and thus eliminates the need for contacts. Further, with ultrafast optical excitation, the method permits one to probe non-equilibrium systems with picosecond to sub-picosecond time resolution. These unique capabilities of the optical-pump/THz-probe spectroscopy have opened up possibilities for the investigation of charge transport phenomena that have remained inaccessible with conventional techniques.

Among the new directions enabled by the optical-pump/THz-probe spectroscopy is the study of carrier transport in wide band-gap insulators. A prototype material of this type is single-crystal sapphire ($\alpha$-$Al_2O_3$), a material of considerable technological and fundamental importance. With respect to the former, sapphire is a widely used material in both electronics and optics, and the characterization of its charge transport properties is of immediate relevance in understanding its electrical [4] and laser-induced [5] breakdown properties. From the fundamental point of view, sapphire is a model ionic crystal and its charge carriers exhibit polaronic behavior, a topic of long-standing theoretical interest [6-12]. In view of the importance of the charge transport in sapphire, there have been several attempts to investigate this phenomenon [13-16]. The wide band gap of the material (8.7 *eV* [17]), which implies a lack of thermally generated carriers, and the absence of electrically active dopants render characterization of charge transport under equilibrium conditions quite difficult. On the other hand, the short carrier lifetime in the material (arising from carrier trapping) also makes it difficult to apply most probing schemes based on the non-equilibrium excitation.

In this work optical-pump/THz-probe spectroscopy is employed to measure conductivity in photo-excited sapphire over a temperature range of 40-350 *K*. Before presenting the main results of our study, we briefly describe the experimental

setup for the measurements in Sect. 2. Optical-pump/THz-probe spectroscopy provides information on the spectral form of conductivity over the THz frequency range, as well as on the dynamics of the process from the dependence of the THz response on the delay of the probe after the ultrafast excitation pulse. In this paper, we are concerned only with the determination of the complex frequency-dependent conductivity (Sect. 3.1), from which the carrier scattering rate is extracted using the Drude model (Sect. 3.2). To clarify the physical nature of the carrier scattering and separate intrinsic and extrinsic contributions, the temperature dependence of the scattering rate is measured in samples with differing levels of impurities. We are able thereby to identify three distinct scattering mechanisms: acoustic-phonon scattering, optical-phonon scattering, and impurity scattering. The phonon scattering processes, being intrinsic to the material, have similar rates in all the samples. Impurity scattering, on the other hand, depends strongly on the properties of the sample under study. In the highest purity samples, impurity scattering was, in fact, found to be absent over the entire temperature range. For a typical optical-grade sample, however, impurity scattering becomes the dominant process at low temperatures (Sect. 3.3 and 3.4). The data that we have obtained on scattering rates also allow one to estimate the electron mobility, as we discuss in Sect. 3.5.

## 2. EXPERIMENTAL

The experimental setup employed in the measurements is depicted schematically in Fig. 1. The laser source (not shown) was an amplified, mode-locked Ti:sapphire system. It provided pulses of 100-*fs* duration at wavelength of 810 *nm*. The pulses had energy of 1 *mJ* and the system was operated at a repetition rate of 1 kHz. Most of the energy (~ 80%) was used to generate third-harmonic pulses centered at 270 *nm* for photo-excitation of the sapphire sample. The remaining pulse energy was utilized for the generation and detection of the THz radiation, which was accomplished, respectively, by optical rectification and electro-optic sampling of the femtosecond laser pulses in ZnTe crystals. A spectral range of 0.3 – 1.5 THz is typically employed to extract the charge transport properties. Further details of the setup can be found in earlier publications [1-3].

In our measurements, charge carriers were created in sapphire through a two-photon absorption process with the third-harmonic photons. The response of the photo-excited carriers was then probed by a THz electromagnetic pulse introduced at a variable delay time. The sapphire samples investigated include several sapphire windows from Meller Optics. In addition, we investigated one high-purity Czochralski-grown sapphire substrate from Union Carbide that had an impurity level of $< 30$ ppm. Most of the experiments were performed with the THz electric field perpendicular to the *c*-axis of the sapphire crystal.

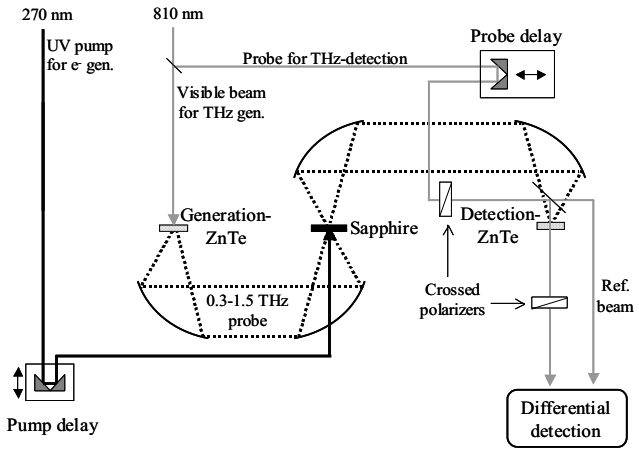


**Fig. 1:** Experimental setup for THz time-domain spectroscopy with a UV pump pulse for the photo-generation of charge carriers. The THz pulses are produced by optical rectification in a ZnTe crystal. Detection of the THz electric field is accomplished by electro-optic sampling with time-synchronized fs laser pulse in a second ZnTe crystal. The sapphire sample is excited with 270 *nm* radiation generated as the third-harmonic of the mode-locked laser.

## 3. RESULTS AND ANALYSIS

### 3.1. Complex conductivity

At each chosen sample temperature, the electric-field waveform, *E(t)*, of the THz pulse transmitted through an unexcited sapphire crystal was recorded by scanning the 810-*nm* femtosecond sampling pulse with respect to the THz pulse. The UV excitation pulse was then introduced to permit the measurement of the change in the THz electric-field waveform, *ΔE(t)*, associated with the photo-excited sample. *ΔE(t)* was obtained by modulating the UV pump pulse and monitoring the differential THz signal for each delay time. In Fig. 2, we illustrate the results of a typical measurement. The THz electric-field waveform *E(t)* transmitted through an unexcited sample is shown as the upper trace. Its photo-induced change *ΔE(t)* is shown as the lower trace. In these measurements, the UV pump fluence was about 20 $J/m^2$ and the delay time between the THz probe and the photo-excitation pulse was about 5 *ps*, a time interval adequate for conduction carriers to reach the thermal equilibrium. The inset in Fig. 2 displays the expected quadratic power dependence of the photo-induced signal on the pump fluence, confirming that the excitation does indeed arise from a two-photon absorption process.

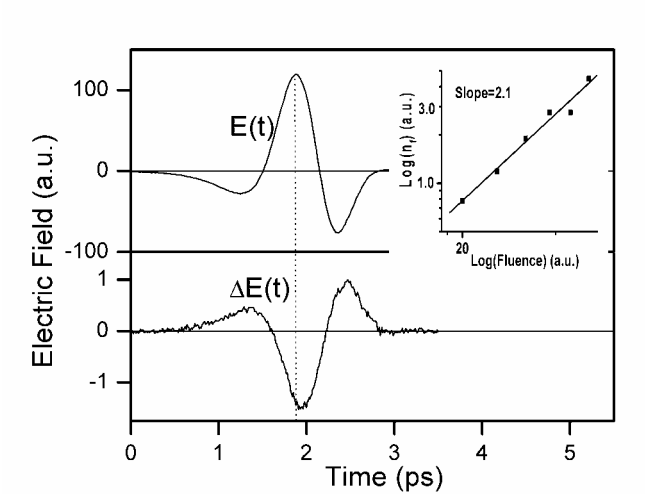


**Fig. 2:** *Upper trace*: THz electric field, *E(t)*, transmitted through a sapphire sample. *Lower trace*: Photo-induced change in the THz waveform, *ΔE(t)*. The UV pump fluence was 20 $J/m^2$ and the pump-probe delay time was 5 *ps*. *Inset:* log-log plot of the power dependence of the photo-generated response. It is fit to power law with an exponent of 2.1.

The pump-induced complex conductivity, $\sigma(\nu) = \sigma'(\nu) + i\sigma''(\nu)$, was then extracted by comparing two electric-field waveforms, *ΔE(t)* and *E(t)*. Following [2], we have

$$\sigma(\nu) = 4\pi i \nu \varepsilon_0 \varepsilon \left[ i\frac{2\pi\nu d}{c/\sqrt{\varepsilon}} - \frac{\sqrt{\varepsilon}-1}{\sqrt{\varepsilon}+1} \right]^{-1} \frac{\Delta E(\nu)}{E(\nu)}. \quad (1)$$

Here *E(ν)* and *ΔE(ν)* are, respectively, the Fourier transforms of the waveforms *E(t)* and *ΔE(t)*; $\varepsilon_0$ is the permittivity of free space; $\varepsilon$ denotes the dielectric function of the unperturbed sample; and $d$ is the thickness of the sample. This relation pertains to the relevant case where the photo-induced change in the THz properties is relatively small. As an example, we show in Fig. 3 (symbols) the photo-induced complex conductivity of a high-purity sapphire crystal at two different temperatures. The excitation and measurement conditions correspond to those of Fig. 2.

### 3.2. Drude model

The measured conductivity in the THz frequency range can be attributed to the photo-generated conduction electrons in the sapphire crystals. The contribution from trapped or bound electrons (or ions) is negligible, since the binding energy is typically much larger than the THz energy. The photo-induced holes also make a contribution. For sapphire this response is relatively small compared with that of the electrons, as indicated in Hall and other measurements [13-15]. This result is also expected from the theoretical prediction of a much larger hole than electron effective mass [18].

Considering only the electron contribution to the frequency-dependent conductivity, the simplest model is given by the Drude form of $\sigma(\nu) = \omega_p^2/(\gamma_o - i2\pi\nu)$. Here $\gamma_0$ denotes the electron scattering rate, and $\omega_p=[ne^2/(\varepsilon_0 m^*)]^{1/2}$ is the plasma frequency, defined in terms of the electron effective mass ($m^*$) and the density of conduction electrons ($n$). This model is seen to fit the experimental data of the complex conductivity well, as shown by solid lines in Fig. 3. The fits yield electron scattering rates of 95 $fs^{-1}$ and 5000 $fs^{-1}$ for sample temperatures of 294 $K$ and 70 $K$, respectively. The plasmon frequency at both temperatures is around 0.9 THz, corresponding to an electron density on the order of $10^{20}$ $m^{-3}$. This latter parameter is, of course, a strong function of the pump excitation fluence. Fits of similar quality to the Drude model have been obtained for all other temperatures in the range of 40 – 350 $K$. In addition, we did not observe any significant variation of the carrier scattering rate with density over the available range of pump fluences (up to 100 $J/m^2$). This result is as expected, considering the relatively low photo-induced electron densities.

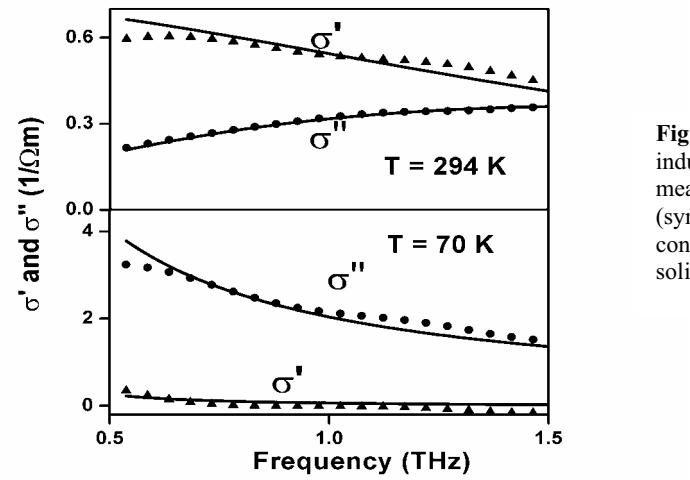


**Fig. 3:** Frequency dependence of the photo-induced complex conductivity for sapphire measured at temperatures of 294 $K$ and 70 $K$ (symbols). The excitation and probing conditions correspond to those of Fig. 2. The solid lines are fits to the Drude model.

**3.3. Temperature dependence of the intrinsic electron scattering rate in sapphire: the large polaron model**

The scattering rate in sapphire has been measured over a range of temperatures from 40 to 350 $K$. The results for a high-purity sapphire substrate (with impurity levels < 30 ppm) are shown as open circles in Fig 4. The scattering rate exhibits a strong dependence on temperature, decreasing by as much as 50 times from 350 $K$ to 40 $K$. In the high-purity sample, the influence of defects is negligible over the entire temperature range, and the observed scattering rate is intrinsic to the material. As we have shown in a previous publication [3], the temperature dependence of the scattering can be understood as a combination of optical- and acoustic-phonon scattering, within a polaron model of the electronic excitations. Briefly, the total scattering rate is obtained by summing over both phonon scattering processes using Mathiessen's law [19]:

$$\gamma_0 = \gamma_{ac}(T) + \gamma_{LO}(T), \tag{2}$$

where $\gamma_{ac}$ and $\gamma_{LO}$ are, respectively, the scattering rates from acoustical and longitudinal optical phonons. In the large polaron model, the conduction electrons are surrounded by a cloud of virtual phonons and form large polarons, quasiparticles that remain mobile but exhibit an enhanced effective mass $m^*$ (relative to the band mass) as they travel through the solid. The scattering rate from LO-phonons is proportional to the optical phonon population. Since the phonon energy exceeds the thermal energy over the range of sample temperatures, this population shows an activated behavior of $\sim e^{-\hbar\omega_{LO}/kT}$, where $\omega_{LO}$ is the frequency of the LO phonon. Acoustic-phonon scattering, on the other hand, depends, following Bardeen and Shockley [20], on the temperature as ~ $T^{3/2}$. The total scattering rate of Eq. (2) for the high-purity sample is then a function of the temperature that involves a superposition of these two functional forms. The data can be fit using just two unknown parameters, the effective mass of the electron (or polaron mass), $m^*$, and the deformation potential, $\varepsilon_{def}$. The other parameters of the model can be obtained from independent measurements of the optical and mechanical properties of sapphire [3]. A fit of the experimental result to the large polaron model of Low and

Pines [7] (solid line in Fig. 4) yields an electron effective mass of 0.3 $m_0$ (corresponding to a band mass of 0.25 $m_0$) and a deformation potential of 19 *eV*. These values are in good agreement with the theoretical estimates from total-energy [21] and band-structure [18] calculations.

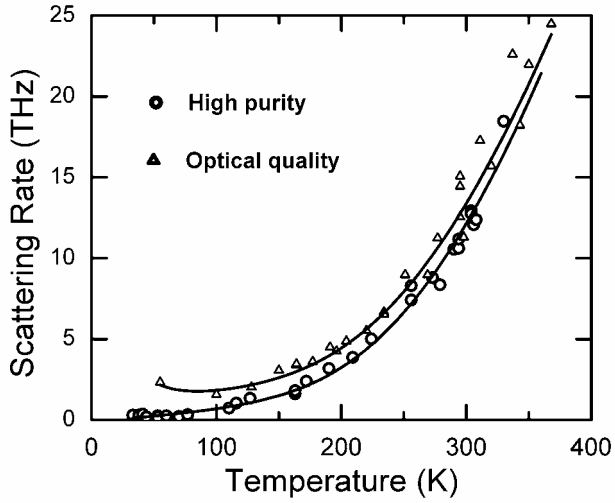


**Fig. 4:** Electron scattering rates in two sapphire crystals of differing purity as a function of temperature, as inferred from a Drude fit to the THz-TDS data. The solid lines are fits to the model described in the text.

### 3.4. Sample-dependent impurity scattering in sapphire

For the high-purity sapphire sample just discussed, the temperature dependence of the scattering rate can be understood entirely in terms of the intrinsic phonon scattering process. Charge transport is not influenced by extrinsic scattering from impurities. In typical optical-quality sapphire windows, impurity scattering is, however, expected to be more significant. In these samples, unlike for the high-purity substrate, we see relatively bright luminescence upon irradiation by the UV pulses. This effect is indicative of the presence of structural defects or chemical impurities, like chromium or titanium, which are known to form color centers responsible for luminescence. The importance of these impurities is further confirmed by a comparison of the dynamics of photo-excited carriers in the different samples. From time-dependent THz probe measurements, we can determine the carrier lifetimes following photo-excitation. For the optical-quality material, a typical carrier lifetime of 20 *ps* was observed; the lifetime in the high-purity sample was found to be close to 200 *ps*. Although the impurities effective in scattering need not be identical to the trapping sites, the lifetime difference suggests an order of magnitude increase in the impurity level of the optical-quality samples compared with the high-purity sample.

In contrast to phonon-scattering mechanism, scattering from ionic impurities actually increases as the temperature decreases. A typical functional dependence for ionic impurity scattering rate with the temperature is $\gamma_{imp}(T) \propto T^{-3/2}$ [19]. The different temperature dependences of impurity and phonon scatterings make the relative importance of these scattering mechanisms change depending on the temperature range in question. This behavior is clearly seen in the temperature-dependent scattering rate of the optical-quality sample (triangles) in Fig. 4. At high temperatures, intrinsic phonon scattering dominates and the scattering rate is very similar to that of the high-purity sample. When the temperature is lowered, however, impurity scattering becomes more important, and the total scattering rate levels off and eventually increases slightly. At about 50 *K*, impurity scattering in the optical-quality sample is more than 10 times greater than that seen in the high-purity sample where phonon scattering dominates.

### 3.5. Electron mobility

With a knowledge of the carrier effective mass $m^*$ and scattering rate $\gamma_0$, we are now in the position to evaluate the carrier mobility using the relation $\mu_e = e/(m^*\gamma_0)$ [19]. For an electron effective mass of $m^* = 0.3\ m_0$ obtained from our analysis of the temperature-dependent scattering rate, we deduce a room-temperature mobility of $\mu_e \sim 600\ cm^2/Vs$ for the high-purity sapphire. This value increases dramatically for decreased temperatures. The mobility reaches 30,000 $cm^2/Vs$ at 40 K, a high value that is often associated with high-mobility semiconductors. The physical origin of the high electron mobility is clear from the discussion above. At low temperatures, the strong contributions from LO phonons

can be completely frozen out, while the acoustic phonon scattering can be strongly reduced. If the sample is also sufficiently pure to have no appreciable impurity scattering, high mobilities can be achieved. For the optical-quality sample of lower purity shown in Fig. 4, we estimated an impurity-limited mobility of ~ 4,000 $cm^2/Vs$.

## 4. CONCLUSIONS

Using the technique of optical-pump/THz-probe spectroscopy, we have studied the complex conductivity in sapphire from photo-generated charge carriers. Sapphire samples with various levels of impurities have been investigated over a temperature range of 40 – 350 *K*. The response of the photo-excited carriers can be described by the Drude model, from which one can deduce important parameters describing charge transport, notably the carrier scattering rate. The temperature dependence of the scattering rates can be understood in terms of large polaron theory, augmented with a contribution from acoustic-phonon scattering. While various samples showed similar scattering rates, and hence mobilities, at room temperature, at cryogenic temperatures clear differences were observed. This behavior reflects the role of impurity scattering at low temperatures in all but the highest purity sample. In addition to these results, two parameters representing the intrinsic properties of the crystal – the electron effective mass and the deformation potential – have been extracted from modeling of the charge transport properties and found to agree well with theoretical predictions. We have also demonstrated that high mobilities can be achieved in wide band-gap crystalline materials having sufficiently low impurity densities. A value of 30,000 $cm^2/Vs$ for the electron mobility has been inferred for high-purity sapphire at a temperature of 40 *K*.

This work was supported primarily by the Nanoscale Science and Engineering Initiative of the National Science Foundation under NSF Award No. CHE-0117752.

## REFERENCES

1. For recent applications, see, for example, M. C. Beard, G. M. Turner, and C. A. Schmuttenmaer, J. Phys. Chem. A **106**, 878 (2002); R. D. Averitt et al. Phys. Rev. Lett. **87**, 017401 (2001); F. A. Hegmann et al. Phys. Rev. Lett. **89**, 227403 (2002); and references therein.
2. E. Knoesel, M. Bonn, J. Shan, and T. F. Heinz, Phys. Rev. Lett. **86**, 340 (2001).
3. J. Shan, F. Wang, E. Knoesel, M. Bonn, T. F. Heinz, Phys. Rev. Lett. **90**, 247401 (2003).
4. J. J. O'Dwyer, *The Theory of Electrical Conduction and Breakdown in Solids and Dielectrics* (Clarendon, Oxford, 1973).
5. N. Bloembergen, IEEE J. Quantum Electron. **QE-10**, 375 (1974).
6. H. Fröhlich, H. Pelzer and S. Zienau, Phil. Mag. 41, 221 (1950) and H. Fröhlich, Advan. Phys. **3**, 325 (1954).
7. F. E. Low and D. Pines, Phys. Rev. **98**, 414 (1955).
8. T. D. Schultz, Phys. Rev. **116**, 526 (1959).
9. Y. Osaka, Progr. Theoret. Phys. (Kyoto) **25**, 517 (1961).
10. L. P. Kadanoff, Phys. Rev. **130**, 1364 (1963).
11. R. P. Feynman, R. W. Hellwarth, C. K. Iddings, and P. M. Platzman, Phys. Rev. **127**, 1004 (1962).
12. Y. Toyozawa, in *Polarons in Ionic Crystals and Polar Semiconductors,* edited by J. T. Devreese (Elsevier, New York, 1972).
13. R. C. Hughes, Phys. Rev. B **19**, 5318 (1979).
14. U. E. Hochuli, Phys. Rev. **133**, A 468 (1964).
15. B. A. Green and M. V. Davis, Trans. Am. Nucl. Soc. **16**, 75 (1973).
16. P. S. Pickard and M. V. Davis, J. App. Phys. **41**, 2636 (1970).
17. J. Olivier and R. Poirier, Surface Sci. **105**, 347 (1981).
18. Y. N. Xu and W. Y. Ching, Phys. Rev. B **43**, 4461 (1991).
19. N. W. Ashcroft and N. D. Mermin, *Solid State Physics* (Saunders College, Philadelphia, 1976).
20. J. Bardeen and W. Shockley, Phys. Rev. **80**, 72 (1950).
21. J.C. Boettger, Phys. Rev. B **55**, 750 (1997) and private communications from J. C. Boettger.